Atmospheric Environment 141 (2016) 388–393

Contents lists available at ScienceDirect

Atmospheric Environment

journal homepage: www.elsevier.com/locate/atmosenv

Satellite observations of ethylene (C_2H_4) from the Aura Tropospheric Emission Spectrometer: A scoping study

Wayana Dolan [a, b], Vivienne H. Payne [a, *], Susan S. Kualwik [c], Kevin W. Bowman [a]

[a] Jet Propulsion Laboratory, California Institute of Technology, Pasadena, CA, USA
[b] Occidental College, Eagle Rock, CA, USA
[c] Bay Area Environmental Research Institute Moffett Field, Moffett Field, CA, USA

HIGHLIGHTS

- Ethylene observed in multiple fire plume observations from Aura TES.
- Ethylene detection limit of 2–3 ppbv for representative boreal fire plumes.
- Spatial averaging needed to detect ethylene from non-fire plume sources.
- Assumptions about ethylene vertical distribution greatly impact VMRs.

ARTICLE INFO

Article history:
Received 3 February 2016
Received in revised form
30 June 2016
Accepted 4 July 2016
Available online 5 July 2016

Keywords:
Ethylene
Tropospheric Emission Spectrometer
Satellite remote sensing

ABSTRACT

We present a study focusing on detection and initial quantitative estimates of ethylene (C_2H_4) in observations from the Tropospheric Emission Spectrometer (TES), a Fourier transform spectrometer aboard the Aura satellite that measures thermal infrared radiances with high spectral resolution (0.1 cm^{-1}). We analyze observations taken in support of the 2008 Arctic Research of the Composition of the Troposphere from Aircraft and Satellites (ARCTAS) mission and demonstrate the feasibility of future development of C_2H_4 into a TES standard product. In the Northern Hemisphere, C_2H_4 is commonly associated with boreal fire plumes, motor vehicle exhaust and petrochemical emissions. It has a short lifetime (~14–32 h) in the troposphere due to its reaction with OH and O_3. Chemical destruction of C_2H_4 in the atmosphere leads to the production of ozone and other species such as carbon monoxide (CO) and formaldehyde. Results indicate a correlation between C_2H_4 and CO in boreal fire plumes. Quantitative C_2H_4 estimates are sensitive to assumptions about the plume height and width. We find that C_2H_4 greater than 2–3 ppbv can be detected in a single TES observation (for a fire plume at 3 km altitude and 1.5 km width). Spatial averaging will be needed for surface-peaking profiles where TES sensitivity is lower.

1. Introduction

Ethylene (C_2H_4) is a hydrocarbon that has both natural and anthropogenic sources. It is formed during biomass burning as well as through processes relating to the petrochemical industry, motor vehicle exhaust, garbage incineration, and biogenic emissions (Sawada and Totsuka, 1986; Gentner et al., 2013). Studies also point to C_2H_4 production in the top layer of the ocean (Seifert et al., 1999; Rudolph and Ehhalt, 1981; Broadgate et al., 1997; Donahue and Prinn, 1993). C_2H_4 has a relatively short lifetime in the troposphere (14–32 h) due to its reactivity with ozone (O_3) and hydroxyl radicals (OH) (Alvarado et al., 2010). These reactions produce very small amounts of several gases of importance to tropospheric chemistry such as carbon monoxide (CO), carbon dioxide (CO_2), and formaldehyde (CH_2O). However, C_2H_4 is primarily known for the role it plays in the formation of ozone, formaldehyde and Criegee intermediates (Sawada and Totsuka, 1986; Gentner et al., 2013; Newland et al., 2015).

Ethylene has previously been detected from space in infrared observations from the Tropospheric Emission Spectrometer (TES), flying on the NASA Aura satellite (Alvarado et al., 2011), the Infrared Atmospheric Sounding Instrument (IASI), flying on the MetOp-A satellite (Clarisse et al., 2011), as well as the Canadian ACE-FTS

* Corresponding author. Jet Propulsion Laboratory, M/S 233-200, 4800 Oak Grove Drive, Pasadena, CA 91109, USA.
E-mail address: vivienne.h.payne@jpl.nasa.gov (V.H. Payne).

http://dx.doi.org/10.1016/j.atmosenv.2016.07.009
1352-2310/

instrument (Herbin et al., 2009). These previous detections were limited to isolated fire plumes. This study demonstrates the identification and initial quantification of C_2H_4 in multiple TES observations and shows a spatial correlation between C_2H_4 and CO in selected boreal fire plumes.

Section 2 provides further background on the spectral signature of C_2H_4 and on the TES observations utilized in this work. Section 3 describes the approach used for detection and quantification of C_2H_4 in TES spectra. Conclusions are presented in Section 4.

2. Background

2.1. Spectral signature of C_2H_4

Our work utilizes the C_2H_4 Q branch at 949 cm^{-1}. To model the feature, we use spectroscopic parameters from the HIgh-resolution TRANsmission molecular absorption (HITRAN) 2000 compilation (Rothman et al., 2003). These parameters are based on laboratory measurements from Cauuet et al., (1990), Pine (1980) and Brannon and Varanasi (1992). C_2H_4 in the 949 cm^{-1} region has not been updated between the HITRAN 2000 compilation and the most recent HITRAN 2012 compilation (Rothman et al., 2013).

Fig. 1 shows optical depth contributions from the C_2H_4 feature at 949 cm^{-1}, alongside other trace gases with spectral features between 940 and 960 cm^{-1}. Optical depths were calculated using the Line By Line Radiative Transfer Model (LBLRTM) (Clough et al., 2005; Alvarado et al., 2013) with temperature and trace gas profiles from the US Standard Atmosphere (Anderson et al., 1986). The C_2H_4 profile was not included in the US Standard Atmosphere and so was taken from model runs associated with the creation of reference atmospheres for the Michelson Interferometer for Passive Atmospheric Sounding (MIPAS) (Remedios et al., 2007). The C_2H_4 profile used in this calculation is representative of expected background concentrations. The strongest absorption features in this spectral region are due to H_2O and CO_2. These features dominate the radiance spectra observed from the satellite (see also Fig. 3).

2.2. Observations from the Aura Tropospheric Emission Spectrometer (TES)

The TES instrument has been flying on the NASA Aura satellite since 2004. TES measures upwelling infrared spectral radiances in the thermal IR range (650-3050 cm^{-1}). The instrument has a variety of observing modes including the global survey, step-and-stare, and transect; each with varying spatial density of observations. The observations used in this research are special observation step-and-stares in the nadir view (Beer et al., 2001). This means that nadir measurements are made every 40 km along the satellite's path for about 50 degrees of latitude (Shephard et al., 2008). Nadir scans have high spectral resolution of 0.06 cm^{-1} (0.1 cm^{-1} apodized) and a footprint of 8 × 5 km^2 (Beer, 2006). Current v006 operational products routinely analyzed by the TES retrieval algorithm (Bowman et al., 2006) include O_3, CO,H_2O, HDO, CH_4, NH_3, HCOOH, CH_3OH, with OCS and PAN to be included in the next release (v007). Atmospheric temperature, surface temperature, surface emissivity, cloud height and cloud effective optical depth (Kulawik et al., 2006) are also routinely retrieved.

This study utilizes step and stare observations that were taken in June and July 2008 in support of the summer phase of the Artic Research of the Composition of the Troposphere from Aircraft and Satellites (ARCTAS) campaign (Jacob et al., 2010). Alvarado et al., (2010) had previously analyzed TES observations from this phase of the campaign, identified TES observations that were affected by fire plumes, and performed back-trajectory calculations to determine the source regions of these plumes. In a subsequent study, Alvarado et al., (2011) identified the first TES observation of C_2H_4 in one these spectra. For this study, we focus on those TES step and stare orbit tracks that had been analyzed by Alvarado et al., (2010).

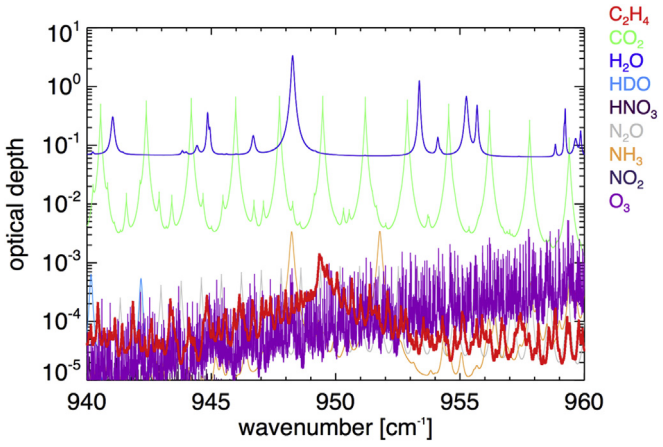

Fig. 1. Optical depth contributions from trace gases in the 940 to 960 cm^{-1} spectral range, assuming a C_2H_4 profile with a tropospheric VMR of 0.04 ppbv. Profiles for all other gases are from the US standard atmosphere.

3. Observations of C_2H_4

3.1. Signals in boreal fire plumes

Alvarado et al., (2010) defined plumes in the TES observations as a set of TES retrievals along a given orbit track between 15th June and 15th July where peak carbon monoxide (CO) exceeded 150 ppbv at 500 mbar and where HYSPLIT back-trajectories (http://ready.arl.noaa.gov.HYSPLIT.php) suggested the observed air masses came from boreal burning regions in Siberia (17 plumes) and Canada (5 plumes). In this work, we started by looking for the spectral signature of C_2H_4 in these previously identified plumes.

Since the signal from C_2H_4 is relatively weak compared to the signal from other molecules in the same spectral region, it is necessary to first perform spectral fits for those other molecules before looking for the C_2H_4 signature. For this work, TES standard atmospheric and surface temperature as well as trace gas (H_2O, HDO, CO_2, O_3, N_2O and NH_3) products, cloud height and cloud effective optical depth were used as inputs to our radiative transfer model. HNO_3 was not retrieved, but was included in the model. Since the spectral region surrounding the 949 cm^{-1} feature is not utilized in the routine TES retrievals, an additional surface emissivity retrieval was performed in spectral windows on either side of the C_2H_4 feature. An example of a resulting brightness temperature residual (observed minus calculated) is shown in Fig. 2.

We consider two parts of the spectrum: one comprising of three spectral points at the location of the peak of the C_2H_4 residual feature (949.3–949.5 cm^{-1} – see Fig. 2), and the other comprised of "no C_2H_4" ranges (938-945 cm^{-1} and 955-962 cm^{-1}). Fig. 3 shows observations from two example plumes, illustrating the variation in the 949.3–949.5 cm^{-1} C_2H_4 signal for individual observations along the TES orbit track, alongside the variation in the 510 mbar CO. In these examples, we see clear indications of spatial correlation between C_2H_4 signals in the spectral residuals and enhanced CO.

If the previous fitting/retrieval steps had accounted for everything in the atmosphere observed by TES, then we might expect the spectral residual to show only random noise. If C_2H_4 is present in a given observation of the atmosphere (scan) at a concentration that would lead to a signal above the instrument noise, then we would

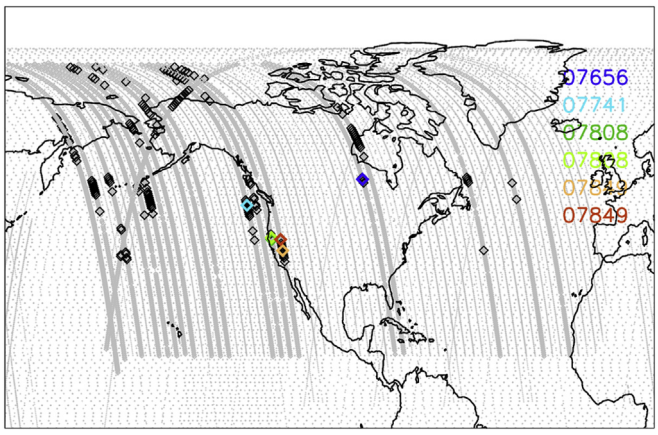

Fig. 2. Small gray points show locations of all TES observations taken during June and July 2008. Larger gray points show the 22 orbit tracks previously analyzed by Alvarado et al., (2010). Black points show the TES scans within those tracks where the TES 500 mbar CO is greater than 150 ppbv. Colored points show locations of the plumes where C2H4 was identified with confidence in the TES observations (see also Table 1).

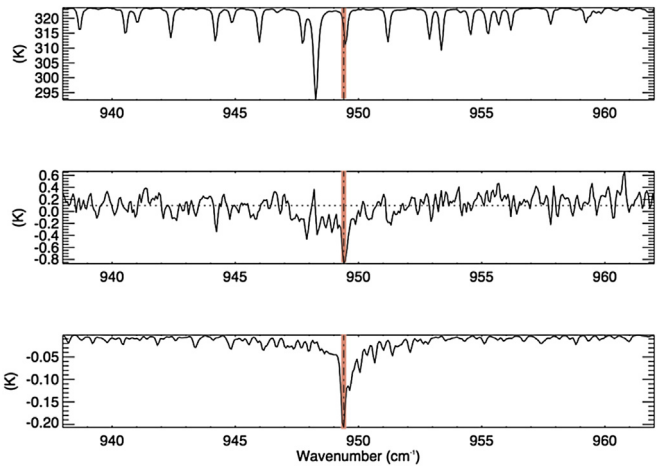

Fig. 3. Example of C_2H_4 signature in a single TES footprint (sounding 7849_001_063), located at 40.199 N, 119.795 W on July 11th, 2008. The position of the C_2H_4 feature is marked by a vertical dashed line in all diagrams. The red highlighted region is the spectral range used during analysis (949.3–949.5 cm^{-1}). Top: TES observed brightness temperature spectrum. Middle: Observed spectrum minus a modeled spectrum without C_2H_4. The horizontal dashed line is the mean of the scan. Bottom: Modeled brightness temperature spectrum with C_2H_4 minus modeled brightness temperature spectrum without C_2H_4. (For interpretation of the references to colour in this figure legend, the reader is referred to the web version of this article.)

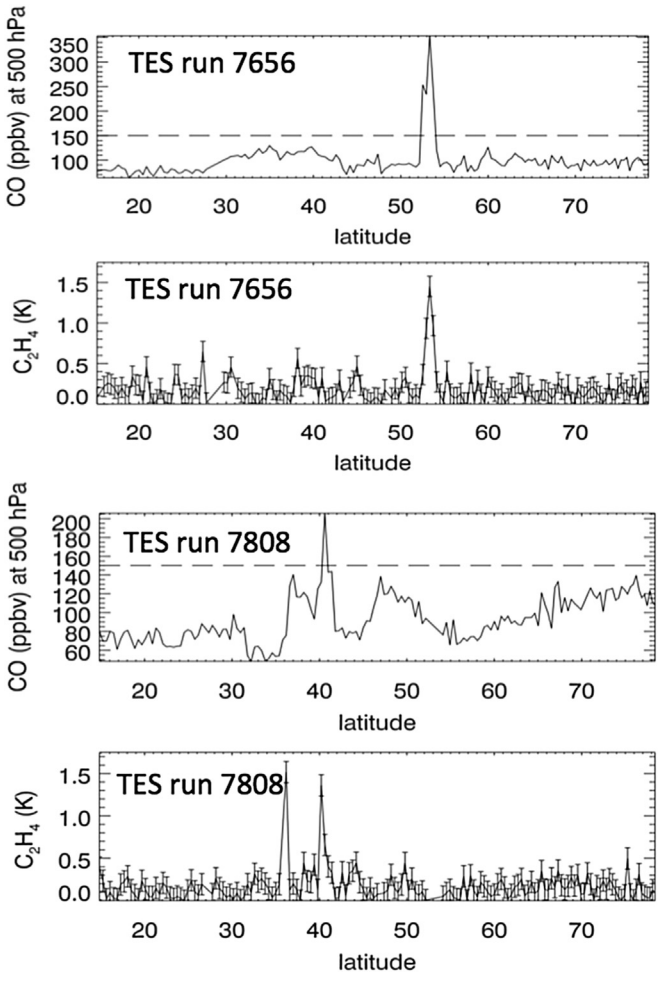

Fig. 4. CO and C_2H_4 plotted against latitude for TES runs 7656 (July 1st, 2008) and 7808 (July 9th, 2008). The dashed lines on the CO plots represent the CO concentration used here to define a CO plume (150 ppbv).

expect to see that signature in the spectral residuals. In practice, the fitting of other variables is imperfect, and the standard deviation of the residuals is generally somewhat larger than the noise.

The ideal residual spectrum for a scan, if fit correctly, should center on zero Kelvin, and, if C_2H_4 is present, should only have a feature where the C_2H_4 feature is located. In practice, the residual spectra are not always ideal. Therefore, we apply some quality flags to the residuals when looking for C_2H_4 signatures. If the standard deviation of the "no C_2H_4" part of the residual spectrum (as defined above) is much greater than the instrument noise, it suggests that something, such as poorly fit temperature or water vapor, is increasing the standard deviation. The ratio of standard deviation of the residual in the no-C_2H_4 part of the spectrum to the instrument noise was calculated for each case. The mean ratio for all scans in the ARCTAS dataset was 1.5, with a standard deviation of 0.4 around this mean. Therefore, if this ratio was greater than 1.9 or less than 1.1, the scan was flagged as bad. If the scan's residual mean does not center on zero, it is also indicative of a poor residual fit. Scans were also flagged as bad if the mean of the scan exceeded 0.9 K or was below −0.6 K. These limits represent the standard deviation of the mean of the means of all scans in the ARCTAS data set. As shown in Fig. 1, CO_2 has a feature at the same spectral location as C_2H_4, as well as other features in the surrounding region of interest. Errors in the temperature retrieval can lead to CO_2 features in the spectral residuals. In principle, systematic errors associated with CO_2 features are distinguishable from the C_2H_4 feature, because all CO_2 features are affected (see Fig. 1). However, we chose to be conservative in screening out scans with a potential conflicting CO_2 signal. We calculated the correlation between each residual spectrum and the result of a constant perturbation to the CO_2 profile. If the r^2 value was greater than 0.1, the scan was flagged as bad.

We define a clear C_2H_4 signal for plumes where the ratio between the signal at the C_2H_4 peak and the standard deviation of the no-C_2H_4 part of the averaged residual is at least 2.0. TES observations from the 22 TES orbit tracks identified by Alvarado et al., (2010) with clear C_2H_4 signals are listed in Table 1 and shown in Fig. 2.

3.2. Feasibility of quantifying C_2H_4

The magnitude of the C_2H_4 signal in the measured spectra depends on the amount of C_2H_4 in the atmosphere, its vertical distribution, and on the details of the surface and atmospheric conditions. The vertical sensitivity of the TES measurement to changes in the C_2H_4 profile at different pressures within the atmospheric column can be assessed by examination of the Jacobian ($\delta R_i/\delta x_j$), which describes the sensitivity of the measured radiance R at wavenumber i to a change in the true atmospheric profile x at pressure level j. Fig. 5 shows the vertical variation of the Jacobian at 949.4 cm^{-1}, the position in the spectrum where the radiances are most sensitive to C_2H_4. The Jacobian is shown for four different C_2H_4 profiles, each with the same peak volume mixing ratio (VMR), but peaking at different altitudes within the troposphere, demonstrating the increased sensitivity of TES radiances to elevated C_2H_4 at higher altitudes/lower pressures.

Due to the magnitude of the C_2H_4 signal compared to the instrument noise (or the standard deviation of the residual fits), we cannot expect to extract information about the vertical distribution of C_2H_4 from the TES radiances. The TES CO observations contain ~1.3 degrees of freedom for signal (DOFS), or independent pieces of vertical information. The vertical resolution of the TES CO profiles is therefore also limited. With better knowledge of the CO profile shape, we might hope to use coincident CO observations to provide some constraints on the vertical characteristics of the plumes. Multi-spectral retrievals of CO from the Measurements of Pollution in the Troposphere (MOPITT), flying on the NASA Terra satellite, use combined information from thermal and short-wave infrared wavelengths to provide improved vertical resolution over land, with ~2 DOFS. However, the Terra orbit does not allow for co-located measurements with TES. In future, short-wave measurements from TROPOMI (due to launch in 2016) and thermal infrared measurements from CrIS on the Suomi-NPP satellite will provide the opportunity for multi-spectral CO retrievals (Fu et al., 2016) that are co-located with C_2H_4 (and other trace gas) measurements. While satellite-based CO retrievals cannot offer the vertical resolution offered by in situ profiling, multi-spectral CO profiles have the potential to offer better vertical information than thermal infrared measurements alone. CO plume heights derived from one of the above would allow reduction in uncertainties of quantitative C_2H_4 estimates.

A range of boreal plumes were observed from aircraft during the ARCTAS campaign. Background C_2H_4 VMRs during ARCTAS were of the order of tens of pptv (Olson et al., 2012). Olson et al. (2012) document fire plumes at altitudes ranging from ground level to 4.5 km. Apel et al., (2012) observed plumes of short-lived trace gases with altitudes ranging from 2 to 6 km. Alvarado et al., (2010) report that the median width of plumes observed from the DC8 aircraft during ARCTAS was 1.5 km, which is equivalent to a half width (σ) of 0.75 km. There were no aircraft underflights for any of the plumes listed in Table 1.

For this study, we assume that the C_2H_4 profile as a function of altitude, vmr(z), can be described by a background VMR plus an additional Gaussian term:

$$\mathrm{vmr}(z) = \mathrm{vmr}_{bkg} + \mathrm{vmr}_{max} e^{-(z-z0)/\sigma}$$

where vmr_{bkg} is the background VMR, vmr_{max} is the peak plume value, z_0 is the altitude of the peak of the plume and σ is the plume half width at half maximum. Profiles that peak at ground level can be accounted for by setting $z_0 = 0$.

The detection limit for C_2H_4 in TES spectra therefore varies based on σ and z_o, as well as the details of the surface and atmospheric temperature. In order to determine approximate detection limits, LBLRTM was run with and without C_2H_4 in order to generate simulated brightness temperature signals for a background of 0.04 ppbv plus plumes with varying values of z_0 and σ, in order to determine the values of vmr_{max} for which the simulated C_2H_4 signal is above 0.15 K (expected value of the standard deviation the spectral residuals for a single TES footprint). Fig. 6 shows the detection limit for different plume altitudes and thicknesses for single TES observations. In these simulations, we also varied the thermal contrast (TC) between the surface and the atmospheric temperature, by shifting the surface temperature. It can be seen that the detection limits for surface-peaking profiles are large, but that the threshold for detection is lower for cases with high thermal contrast. These detection limits can be decreased by spatial averaging.

In order to evaluate VMR values that are representative of the boreal plumes listed in Table 1, we assumed a background of 0.04 ppbv with a Gaussian plume, with a plume height of 3 km and full width half maximum of 1.5 km. We performed iterative forward model runs using LBLRTM to determine the peak VMR that would match the observed C_2H_4 signal in the averaged residual for the plume. In each case, the initial guess value of vmr_{max} was set to

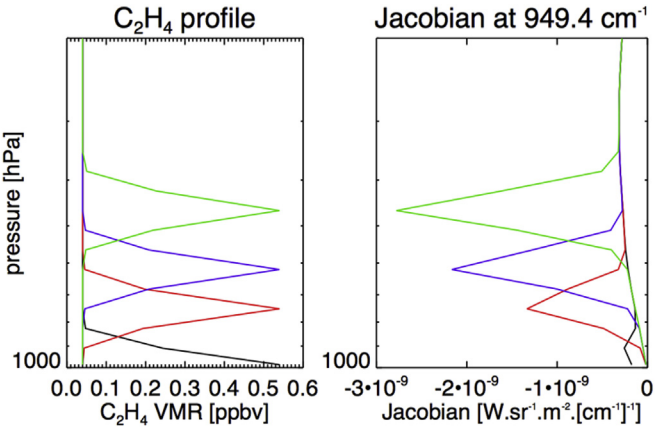

Fig. 5. Left: four hypothetical profiles with identical peak VMRs and varying plume height. Right: Jacobians (calculated with LBLRTM) demonstrating the increased sensitivity of TES radiances to elevated C_2H_4 at higher altitudes and lower pressures.

Table 1
TES observations of C_2H_4 in boreal fire plumes in June/July 2008. Plume source identification is from Alvarado et al., (2010). Estimated C_2H_4 values are based on the assumption of a gaussian distribution of C_2H_4 in the vertical, centered at 3.0 km, with a full-width at half-maximum of 1.5 km (σ = 750 m).

TES sounding	Date	Latitude [degrees]	Location of source fire	C_2H_4 signal [K]	Estimated peak VMR (with uncertainty) [ppbv]	Max. TES CO value [ppbv]
7656_0001_096	2008-07-01	53.3	Canada	1.56	25 (14)	1043
7741_0001_082	2008-07-05	47.6	Siberia	0.44	18 (14)	542
7808_0001_063	2008-07-09	40.2	Siberia	1.38	24 (15)	1140
7808_0001_064	2008-07-09	40.6	Siberia	0.73	12 (7)	417
7849_0001_057	2008-07-11	37.8	Siberia	0.40	5.5 (3.7)	536
7849_0001_063	2008-07-11	40.2	Siberia	0.94	8.6 (4.3)	474

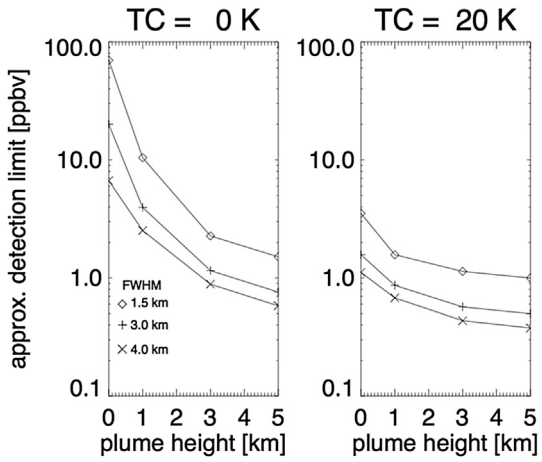

Fig. 6. Detection limits for C_2H_4 in an individual TES observation, based on varying thermal contrasts (TC), plume heights, and full plume widths at half maximum (FWHM). A surface-peaking profile with FWHM would be broadly consistent with a boundary layer altitude of 2 km.

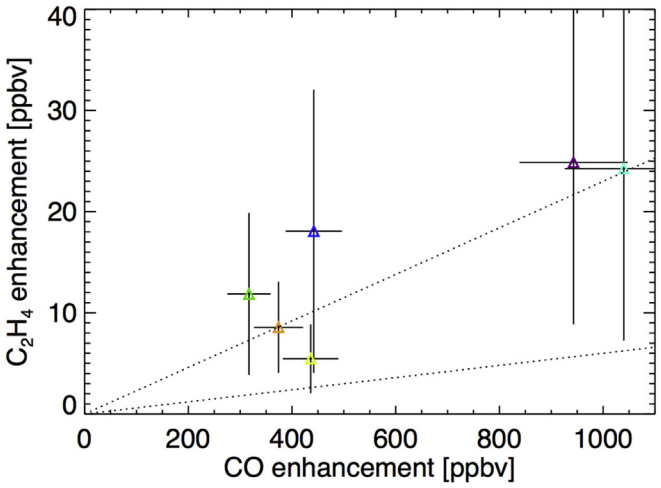

Fig. 7. ΔC_2H_4 and ΔCO enhancement from the TES observations listed in Table 1. Dotted lines show the range of $\Delta C_2H_4/\Delta CO$ enhancement ratios for boreal fires reported by Akagi et al., (2011). Colors of the points correspond to the colors in Fig. 2.

0.5 ppbv. Within 3 iterations, the inferred value of vmr_{max} converged to the values shown in Table 1, in that the inferred value did not change by more than 0.1 ppbv between iterations 2 and 3. Profiles of temperature and other trace gases were taken from the TES retrievals for a scan in the middle of the latitude range of each plume. Values are reported in Table 1. In order to estimate uncertainties on these C_2H_4 values, we also determined the inferred peak VMR using a plume height of 5 km instead of 3 km, a plume FWHM of 3 km instead of 1.5 km and the uncertainty associated with the standard deviation of the non-C_2H_4 spectral regions. These three error terms were added in quadrature to give the uncertainty estimates provided in Table 1. For these plume cases where the signal is large compared to the instrument noise and the standard deviation of the residual, the total uncertainty arises mainly from the uncertainty in plume width. The total error bars are large compared to the magnitude of the estimated VMRs.

As stated previously, aircraft underflights were not available to validate the C_2H_4 VMR estimates for these plumes. However, a crude validation can be provided using previous measurements of emission ratios from boreal fires from laboratory and airborne studies (Akagi et al., 2011). These previous estimates suggest $\Delta C_2H_4/\Delta CO$ enhancement ratios ranging between 0.006 and 0.023 ppb/ppb.

In the absence of co-incident in situ C_2H_4 profile observations, we can use this $\Delta C_2H_4/\Delta CO$ enhancement ratio value as a type of validation. In order to obtain a representative CO value, we average the TES CO for the 3 levels around the peak observed CO profile. We assume a background CO VMR of 80 ppbv. TES CO mixing ratios have an uncertainty of approximately 10% (Luo et al., 2010), which would equate to 15–100 ppbv for these boreal fire plume cases. ΔC_2H_4 and ΔCO enhancement from the TES observations listed in Table 1 are shown in Fig. 7. From this figure, we would conclude that there is, as would be expected, a general tendency towards higher C_2H_4 values for plumes with higher CO. The lower bounds of the TES error bars do all lie within the Akagi et al. range. However, the C_2H_4 values from the TES analysis are higher than those that would be inferred by using the enhancement ratios from Akagi et al., (2011), This is not the direction of disagreement that would be expected. In general, we would have expected that the enhancement of C_2H_4 relative to CO observed in satellite measurements would be lower than that observed from in situ measurements, since the lifetime of C_2H_4 is shorter than that of CO and we would expect that the satellite measurements would tend to sample older plumes than the in situ studies. At the current time, it is not known whether this discrepancy is particular to the small number of cases examined in this study, or whether it is a wider issue that would apply to all observations of C_2H_4 in plumes from TES and/or other thermal infrared instruments.

In addition to the fire plume examples discussed above, we did see cases over the remote Atlantic in the 20N-35N latitude range where spectral residuals at the peak of the C_2H_4 feature were higher than the residual standard deviation, but the TES CO was not enhanced, indicating that these are not fire plume cases. Based on the approximate detection limits shown in Fig. 4, it would be difficult to make the argument for confident detection on the basis of single TES footprints. Assuming that remote ocean cases would have C_2H_4 profiles that peak at the surface, and assuming profiles with a Gaussian half-width equal to a boundary layer height of ~2 km (full width of 4 km in Fig. 4), surface VMR values > 1 ppbv would be required for single footprint detection. However, spatial averaging over the order of 50–100 ocean cases provides greater confidence in the signal by reducing the standard deviation in the residuals by a factor of 2–3. The standard deviation does not scale as the square root of the number of cases here, as it would for pure instrument noise, due to the presence of errors in the residual fits associated with temperature, water vapor and other trace gases. Nonetheless, with a reduction in the standard deviation of the residuals, the detection limit for C_2H_4 is lowered by a corresponding factor and the TES residuals show identifiable C_2H_4-shaped features. Previous studies (Rudolph and Ehhalt, 1981; Seifert et al., 1999) have measured C_2H_4 over the Atlantic Ocean, with surface volume mixing ratios of up to 0.51 ppbv. This indicates that TES has the potential to offer information about smooth variation of C_2H_4 on large spatial scales in addition to observations of fire plumes.

We also note here that there are other thermal infrared sounders, such as the Atmospheric Infrared Sounder (AIRS) on the Aqua satellite, the Cross-Track Infrared Sounder (CrIS) on the Suomi-NPP satellite and the Infrared Atmospheric Sounding Instruments on the MetOp satellite series, that measure spectrally-resolved radiances in the C_2H_4 spectral range, but offer denser spatial coverage. Denser spatial coverage would mean that the same number of observations would be obtained in a smaller area, although further work would be require to examine the impact of the different spectral resolution and noise characteristics of those other instruments on C_2H_4 detection and quantification.

4. Conclusions

We show that C_2H_4 is detectable in multiple TES scans, and therefore acts as a proof of concept for the feasibility of C_2H_4 development into a TES standard product. We also show a spatial correlation between C_2H_4 and CO in selected fire plumes. Estimated values of C_2H_4 in six fire plumes examined here are generally high compared to values inferred from previous aircraft studies, although our values agree with the previous studies within the error bars on the TES estimates. This study demonstrates the importance of assumptions about vertical distribution of C_2H_4 within the atmosphere in determining absolute values for C_2H_4 VMRs, as TES has markedly greater sensitivity to C_2H_4 in the free troposphere than to C_2H_4 close to the ground. Co-located multi-spectral CO retrievals could provide this vertical information. The detection limit is strongly dependent on the assumed vertical distribution of C_2H_4 as well as the thermal contrast between the atmosphere and the surface. The detection threshold can be lowered with spatial averaging. Results suggest that evaluation of large-scale variations in C_2H_4 for conditions outside fire plumes is possible from TES (and potentially from other thermal infrared instruments). The development of an optimal estimation C_2H_4 algorithm, with appropriate prior constraints and associated prior and posterior error analysis will be the topic of future work. Routine processing of C_2H_4 retrievals from TES in an optimal estimation framework would provide a global, multi-year dataset with the associated error estimates and sensitivity diagnostics needed to enable the use of this data to provide improved constraints on global chemical models.

Acknowledgements

The research was carried out at the Jet Propulsion Laboratory, California Institute of Technology, under a contract with the National Aeronautics and Space Administration. We would like to thank Matthew Alvarado (AER) for helpful discussions on enhancement ratios, and Dylan Millet (University of Minnesota) for supplying C_2H_4 fields from a global chemical model, which were not used in this paper but were helpful in the overall consideration of background profile shapes for C_2H_4.

References

Akagi, S.K., Yokelson, R.J., Wiedinmyer, C., Alvarado, M.J., Reid, J.S., Karl, T., Crounse, J.D., Wennberg, P.O., 2011. Emission factors for open and domestic biomass burning for use in atmospheric models. Atmos. Chem. Phys. 11, 4039–4072. http://dx.doi.org/10.5194/acp-11-4039-2011.

Alvarado, M.J., et al., 2013. Performance of the Line-by-Line Radiative Transfer Model (LBLRTM) for temperature, water vapor, and trace gas retrievals: recent updates evaluated with IASI case studies. Atmos. Chem. Phys. 15, 6687–6711.

Alvarado, M.J., Cady-Pereria, K.E., Xiao, Y., Millet, D.B., Payne, V.H., 2011. Emission ratios for ammonia and formic acid and observations of peroxy acetyl nitrate (PAN) and ethylene in biomass burning smoke as seen by the tropospheric emission spectrometer (TES). Atmosphere 2, 633–644. http://dx.doi.org/10.3390/atmos2040633.

Alvarado, M.J., et al., 2010. Nitrogen Oxides and PAN in plumes from boreal fires during ARCTAS-B and their impact on ozone: an integrated analysis of aircraft and satellite observations. Atmos. Chem. Phys. 10, 9739–9760. http://dx.doi.org/10.5194/acp-10-9739-2010.

Anderson, G.P., et al., 1986. AFGL Atmospheric Constituent Profiles (0-120 Km), AFGL-TR-86-0110, Air Force Geophysical Laboratory.

Apel, E.C., et al., 2012. Impact of the deep convection of isoprene and other reactive trace species on radicals and ozone in the upper troposphere. Atmos. Chem. Phys. 12, 1135–1150.

Beer, R., 2006. TES on the Aura mission: scientific objectives, measurements, and analysis overview. IEEE Trans. Geosci. Remote Sens. 44, 1102–1105.

Beer, R., et al., 2001. Tropospheric emission spectrometer for the earth observing System's Aura satellite. Appl. Opt. 44, 2356–2367.

Bowman, K.W., et al., 2006. Tropospheric emission spectrometer: retrieval method and error analysis. IEEE Trans. Geosci. Remote Sens. 44, 1297–1307.

Brannon Jr., J.F., Varanasi, P., 1992. Tunable diode laser measurements on the 951.7393cm^{-1} line of $^{12}C_2H_4$ at planetary atmospheric temperatures. JQSRT 47, 237–242.

Broadgate, W.J., Liss, P.S., Penkett, S.A., 1997. Seasonal emissions of isoprene and other reactive hydrocarbon gases from the ocean. Geophys. Res. Lett. 24, 2675–2678. http://dx.doi.org/10.1029/97GL02736.

Cauuet, I., et al., 1990. Extension to third-order Coriolis terms of the analysis of v 10, v 7, and v 4 levels of ethylene on the basis of Fourier transform and diode laser spectra. J. Mol. Spectrosc. 139, 191–214.

Clarisse, L., R'Honi, Y., Coheur, P., Hurtmans, D., Clerbaux, C., 2011. Thermal infrared nadir observations of 24 atmospheric gases. Geophys. Res. Lett. 38.

Clough, S.A., et al., 2005. Atmospheric radiative transfer modeling: a summary of the AER codes. J. Quant. Spectrosc. Radiat. Transf. 91, 233–244.

Donahue, N.M., Prinn, R.G., 1993. In-situ nonmethane hydrocarbon measurements on SAGA-3. J. Geophys. Res. 98, 16915–16932.

Fu, D., Bowman, K.W., Worden, H., Natraj, V., Yu, S., Worden, J.R., Veefkind, P., Aben, I., Landgraf, J., Strow, L., Han, Y., 2016. High resolution tropospheric carbon monoxide profiles retrieved from CrIS and TROPOMI. Atmos. Meas. Tech. 9, 2567–2579.

Gentner, D.R., Worton, D.R., Isaacman, G., Davis, L.C., Dallmann, T.R., Wood, E.C., Herndon, S.C., Goldstein, A.H., Harley, R.A., 2013. Chemical composition of gas-phase organic carbon emissions from motor vehicles and implications for ozone production. Environ. Sci. Technol. 47 (20), 11837–11848. http://dx.doi.org/10.1021/es401470e.

Herbin, H., Hurtmans, D., Clarisse, L., Turquety, T., Clerbaux, C., Rinsland, C.P., Boone, C., Bernath, P.F., Coheur, P.F., 2009. Distributions and seasonal variations of tropospheric ethylene (C_2H_4) from Atmospheric Chemistry Experiment (ACE-FTS) solar occultation spectra. Geophys. Res. Lett. 36 (L04801) http://dx.doi.org/10.1029/2008GL036338.

Jacob, D., Crawford, J.H., Maring, H., Clarke, A.D., Dibb, J.E., Ferrare, R.A., Hosteler, C.A., Russell, P.B., Singh, H.B., Thompson, A.M., Shaw, G.E., McCauley, E., Penderson, J.R., Fisher, J.A., 2010. The arctic research of the composition of the troposphere from aircraft and satellites (ARCTAS) mission: design, execution and first results. Atmos. Chem. Phys. 10, 5191–5212.

Kulawik,, S.S., Worden, J., Eldering, A., Bowman, K., Gunson, M., Osterman, G.B., Zhang, L., Clough, S., Shephard, M.W., Beer, R., 2006. Implementation of cloud retrievals for Tropospheric Emission Spectrometer (TES) atmospheric retrievals: part 1. Description and characterization of errors on trace gas retrievals. J. Geophys. Res. 111, D24204. http://dx.doi.org/10.1029/2005JD006733.

Luo, M., et al., 2010. Interpretation of Aura satellite observations of CO and aerosol index related to the December 2006 Australia fires. Remote Sens. Environ. 114, 2853–2862.

Newland, M.J., et al., 2015. Kinetics of stabilized Criegee intermediates derived from alkene ozonolysis: reactions with SO2, H2O and decomposition under boundary layer conditions. Atmos. Chem. Phys. 4076.

Olson, J.R., et al., 2012. An analysis of fast photochemistry over high northern latitudes during spring and summer using in-situ observations from ARCTAS and TOPSE. Atmos. Chem. Phys. 12, 6799–6825.

Pine, A.S., 1980. Tunable Laser Survey of Molecular Air Pollution. Final Report, NSF/ASRA/DAR. Massachusetts Inst. of Tech., Lexington (USA), pp. 78–24562. Lincoln Lab.

Remedios, J.J., et al., 2007. MIPAS reference atmospheres and comparisons to V4.61/V4.62 MIPAS level 2 geophysical data sets. Atmos. Chem. Phys. 7, 9973–10017.

Rothman, L.S., et al., 2003. The HITRAN molecular spectroscopic database: edition of 2000 including updates through 2001. J. Quant. Spectrosc. Radiat. Transf. 82, 5–44.

Rothman, L.S., et al., 2013. The HITRAN 2012 molecular spectroscopic database. J. Quant. Spectrosc. Radiat. Transf. 130, 4–50.

Rudolph, J., Ehhalt, D.H., 1981. Measurements of C_2-C_5 hydrocarbons over the North atlantic. J. Geophys. Res. 86, 11959–11964.

Sawada, S., Totsuka, T., 1986. Natural and anthropogenic sources and fate of atmospheric ethylene. Atmos. Environ. 20, 821–832.

Seifert, R., Delling, N., Richnow, H.H., Kempe, S., Hefter, J., Michaelis, W., 1999. Ethylene and methane in the upper water column of the subtropical Atlantic. Biogeochemistry 44, 73–91.

Shephard, M.W., et al., 2008. Tropospheric Emission Spectrometer nadir spectral radiance comparisons. J. Geophys. Res. 113 (D15S05) http://dx.doi.org/10.1029/2007JD008856.